International Journal of Engineering & Technology, 7 (4.36) (2018) 354-362

International Journal of Engineering & Technology

Website: www.sciencepubco.com/index.php/IJET

Research paper

Band Gap Modification of Tio_2 Using Solid State Reaction with Hydrides in Argon Atmosphere

Saad Sh. Al-Omary [1], Laith A. Algharagholy [2], Mohsin E. Al-Dokheily [3]

[1]Chemistry Department, College of Science, University of Dhi-Qar, Nasiriyah, Dhi-Qar, Iraq.
[2]Department of Natural Science, College of Basic Education, University of Sumer, Refayee, Dhi-Qar, Iraq.
[3]Chemistry Department, College of Science, University of Dhi-Qar, Al Islah , Dhi-Qar, Iraq.
Corresponding author: Saad Sh. Al-Omary
Nasiriyah, Dhi-Qar, Iraq
**Corresponding author E-mail: saad.sh_chem@sci.utq.edu.iq*

Abstract

TiO_x (x<2) nanoparticles have been synthesized by solid state reaction between as-prepared TiO2 nanoparticles and $NaAlH_4$, KBH_4 as a reducing agents in argon atmosphere at two temperature 600 ºC and 850 ºC . the X-ray diffraction patterns of reduced TiO_2 shows a peak shift and broadening which attributed to the lattice contraction after reduction treatment. AFM images confirm that the surface roughness of reduced TiO_2 were larger than unmodified TiO_2 nanoparticles due to the formation of oxygen vacancies. UV-Vis spectroscopy measurements revealed that the reduced TiO2 nanoparticles have an absorption edge lies in the visible region from the electromagnetic radiations with lower band gap. EDS spectra indicate that the as-prepared and reduced TiO_2 nanoparticles have a high degree of purity and the acquired results confirm formation nonstoichiometric (TiO_{2-x}) with oxygen deficient.

Keywords: *TiO2, band gap , reduction , solid state , DFT, SIESTA*

1.Introduction

Titanium dioxide TiO_2 has been studied intensively, this is because of its chemical and biological inertness, high photocatalytic efficiency, environmental tolerance, large stability, and low cost [1]. Many efforts have been made to modify TiO_2 activity for degradation organic compounds , water splitting and for oxygen or hydrogen production [2,3]. Typically, the shape, size, crystal phase, crystallinity ,surface structure and defects represent the important parameters of TiO_2 , which are related strongly to its properties[4-8]. However, pure TiO_2 is not a good material for practical applications because of the wide band gap (3.2 eV for anatase phase, and 3.0 eV for rutile phase), this mean it can be activated only under the UV radiations which make about 5% from the total solar radiation [9].There are many treatments to improve the photocatalytictic activity of TiO_2 in visible light range, this methods include doping titanium dioxide with metal ions such as (Cu, Fe, V), and nonmetals such (C,N), and with rare earth elements and introducing defects into its structure [10].

Oxygen vacancy is one of the most important and is believed to be the common defect in many metal oxides, which has been investigated intensively by experimental characterizations and theoretical calculations.

Reduced TiO_2 nanoparticles (TiO_{2-x}), that contains oxygen vacancy or Ti^{+3} has been confirmed to show visible light absorption[11]. Yet it was thought that the introduced localized oxygen vacancy states that have energies of 0.75 to 1.18 eV below the conduction band minimum of TiO_2 nanoparticles are less than the redox potential for evolution of hydrogen, which, in combination with the little electron mobility in the bulk region related to this localization, makes the photocatalytic activity of the reduced TiO_2 insignificant [12]. However, theoretical calculations estimate that a vacancy band of electronic states induced by high vacancy concentration can be a just below the conduction band[13]. However, these results show that it is possible to construct visible-light responsive TiO_2 through introducing oxygen vacancy or Ti^{+3}[14].

Self-doping of TiO_2 can be done using different reductants such as hydrogen gas, aluminium powder ,metallic zinc, sodium borohydride , diethylene glycol , carbon monoxide and so for.[15-20].

in this work , TiO_2 nanoparticles was prepared using a well known sol-gel method, then, the band gap of as-prepared TiO_2 nanoparticles were modified using solid state reaction method in inert atmosphere with new reductant materials. These modified TiO_2 nanoparticles having lower band gap as compared with unmodified TiO_2 .

2.Experimental

2.1 Materials

The chemicals used in this work are (titanium tetraisopropoxide 97% , sodium aluminum hydride 90% , Potassium borohydride 98%) purchased from sigma Aldrich , (Isopropanol 90% , Nitric acid 60%) purchase from BDH, the chemicals used in this work were of analytical reagent grade.

2.2 Preparation TiO2 nanoparticles

Titanium dioxide nanoparticles were synthesized using sol-gel method , solution of titanium tetraisoprppoxide and isopropanol (5 ml isopropanol , 5 ml titanium isopropoxide) was added gradualy to 200 ml of deionzed water at pH 5 , the rate of addition is 2 ml / min. When the addition is completed ,The mixture was kept 2 hours with continuous dynamic mixing at room temperature to reach the completion of hydrolysis. Then, the solution of transparent colloidal was left for 24 hours to complete aging , after that , filtered and dried for two hours at 90 ^oC . For comparison, the resulted powder calcined for 4 hours in air atmosphere at 600 ^oC , denoted A-TiO_2 and at 850^oC, denoted R-TiO_2 to obtain anatase and rutile phase respectively.

Modified TiO_2 was prepared using solid state reaction of uncalcined TiO_2 with sodium aluminum hydride and potassium borohydride. 0.5 mole of $NaAlH_4$ and KBH_4 mixed with 1 mole of TiO_2 separately. Mixed and grounded carefully and placed in quartz tube furnace and calcined in argon atmosphere at 600^oC and 850 ^oC, Finally, the products were allowed to cool at room temperature. To remove unreacted NaAlH and KBH4, the resulted powder washed with deionized water and ethanol several times. The resulted powder denoted T-Na-600, T-Na-850, T-K-600, T-K-850, where Na and K represent NaAlH4 ,KBH4 respectively , 600 and 850 represent calcinations temperatures. The conditions of solid state reactions experiments illustrated in table (1).

2.3 Synthesis of modified TiO2 nanoparticles

Table (1) solid state reaction conditions

reactants	Mole ratio	Temperature ^oC	Reaction time
TiO_2 + $NaAlH_4$	1 : 0.5	600	1 hour
TiO_2 + $NaAlH_4$	1 : 0.5	850	1 hour
TiO_2 + KBH_4	1 : 0.5	600	1 hour
TiO2 + KBH_4	1 : 0.5	850	1 hour

2.4 Characterization

X-ray diffraction patterns of prepared and modified TiO2 were analyzed using Shimadzu X-Ray Diffractometer XRD 6000 with Cu Kα (λ= 0.15405 nm). Atomic force microscopy (AFM) images were measured using Advanced angstrom (AA3000) Model made in USA. Scanning electron microscopy (SEM) and energy dispersive spectroscopy (EDX) using Multi-Function Scanning Electron Microscope Model als 2300 Angstrom. The UV-Vis absorption spectra were recorded using Shimadzu UV-Visible 1800 spectrophotometer.

3.Results and discussion

The X-ray diffraction (XRD) is performed to identify the Changes of the crystalline phase of prepared and modified TiO2 nanoparticles. As shown in Figs. (1-2) and table(2), there were no other diffraction peaks, which indicated that the samples were pure, all the diffraction peaks related only to Tio2 Anatase (JCPDS Card No. 21–1272)and Rutile phases(JCPDS Card No. 21–1276). However, there is a significant peaks broadening and shifting in 2θ values to higher values after reduction reaction due to formation oxygen vacancies and lattice strains (21,22). The crystallite size of prepared and modified Tio2 calculated using Scherrer equation(23):

$D = 0.9 \lambda / \beta \cos\theta$ where

D = crystallite size

β = full width at half maximum intensity

θ = diffraction angle

0.9 = shape factor

Table 2: crystallite size and cell parameters obtained from XRD spectra

compound	Miller indices	2θ degree	FWHM cm^{-1}	D nm	Cell parameters ^oA	Cell volume $^oA^3$
A-TiO2	1 0 1	25.28	0.4324	18.62	a =3.779 c =9.665	138.024
R-TiO2	1 1 0	27.43	0.2104	38.43	a =4.549 c =2.946	62.174
T-K-600	1 0 1	25.40	0.4990	16.14	a =3.761 c =9.628	136.189
T-K-850	1 1 0	27.58	0.2770	29.20	a =4.570 c =2.937	61.338
T-Na-600	1 0 1	25.45	0.5212	15.45	a =3.753 c=9.621	135.511
T-Na-850	1 1 0	27.63	0.2993	27.03	a =4.562 c=2.933	61.041

As shown in table(2) , the cell parameters and cell volume of modified tio2 lower than that as-prepared tio2, also, we can note that the crystallite size of modified tio2 smaller than that for reduced tio2 which is derived from oxygen vacancies induced lattice strains and slightly reduced crystal size and lattice contraction (24,25,26). Moreover, the lattice contraction in case of T-Na-600 larger than that of T-K-600, similarly, the contraction in the T-Na-850 is larger than T-K-850 this is because NaAlH4 represent a stronger reducing agent as compared with KBH4.

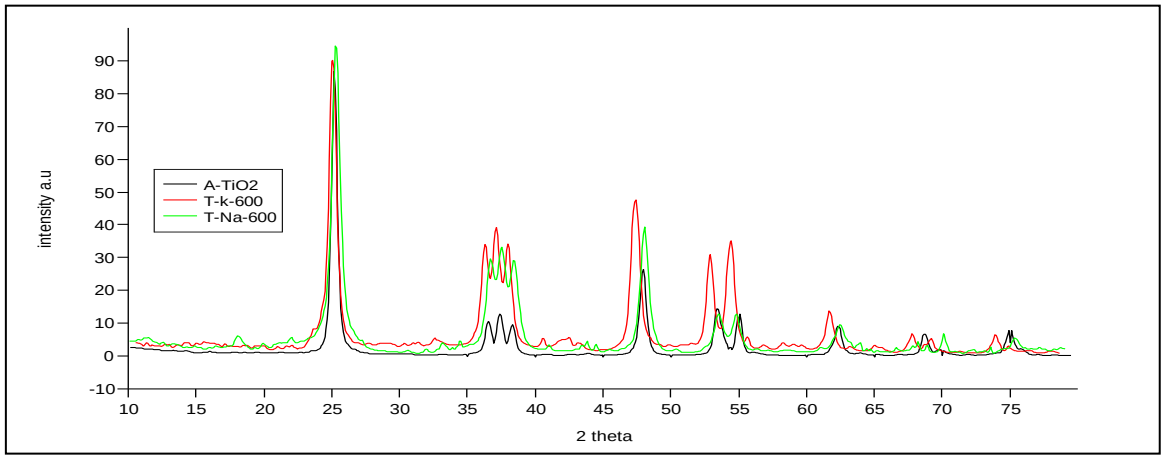

Figure 1 : xrd patterns of A-TiO2 , T-K-600 , T-Na-600

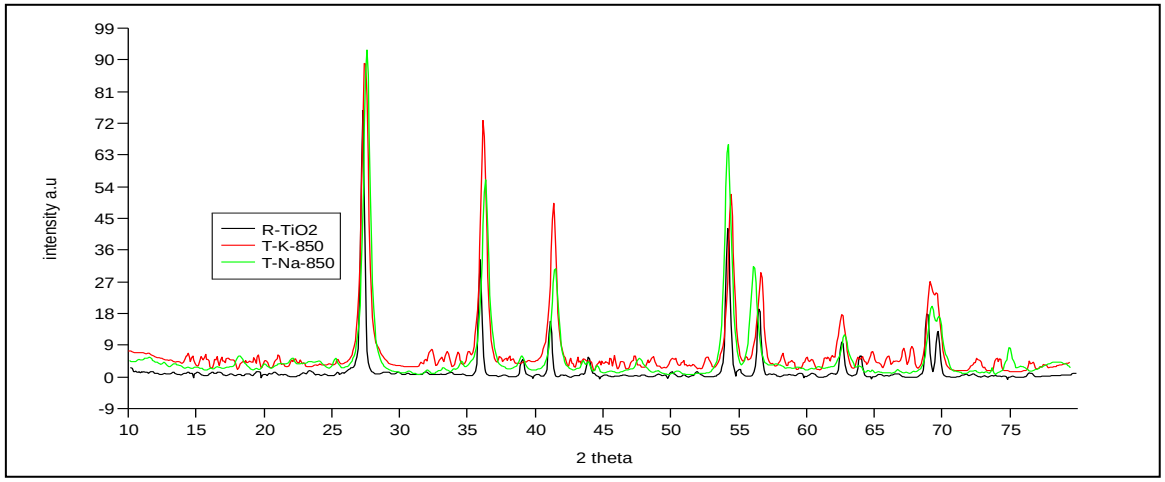

Figure 2 : xrd patterns of R-TiO2 , T-K-850 , T-Na-850

The optical properties of the TiO2 nanoparticles were characterized Using UV-vis spectroscopy, figure (3) illustrate the absorption spectra , One of the most successful methods for determining the bandgap energy is Tauc plot, The bandgap energy (Eg) can be calculated using the following equation(27):

$\alpha h\nu = A(h\nu - E_g)^{1/2}$

by extrapolating the tangent line of the (αhν)1/2 plot drown vs. hν we can obtain the Eg values of as-prepared and modified tio2. As shown in figure(4) and table (3), the band gap was approximately 3.2 ev and 2.9 ev for A-TiO2 and R-TiO2 respectively.

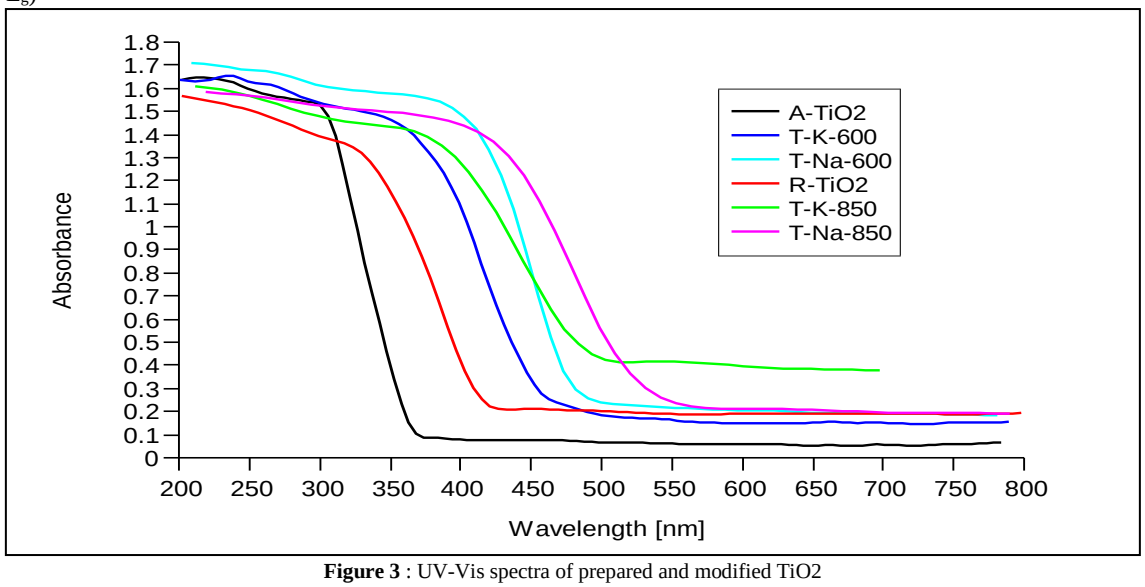

Figure 3 : UV-Vis spectra of prepared and modified TiO2

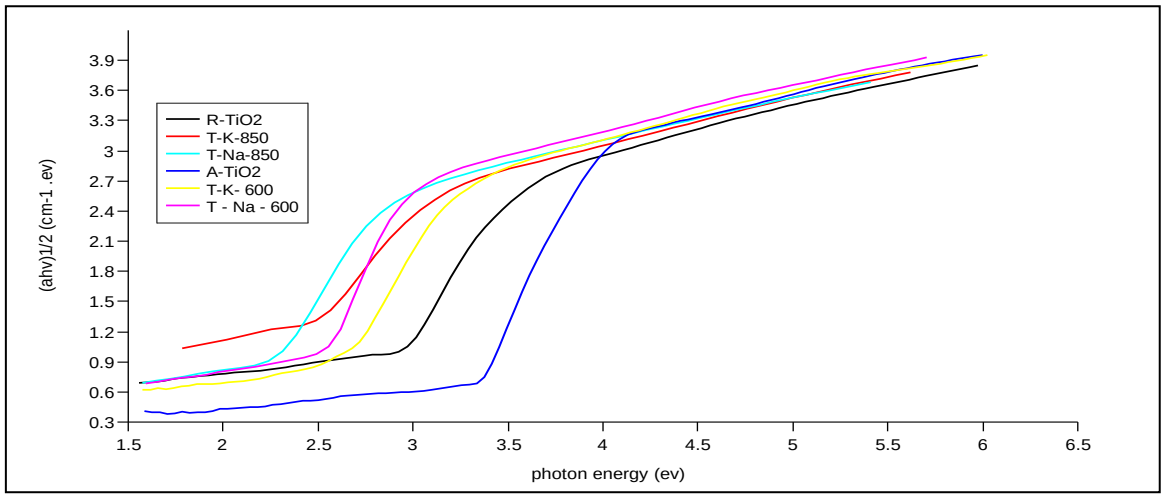

Fig. 4 : Tauc plot of as-prepared and modified TiO2

On the other hand, reduction treatment shift the absorption edge from the ultraviolet to visible region and the band gap become smaller, the band gap of T-Na-600, T-Na-850 more effected by reduction treatment and therefore have lower band gap. however, the introducing oxygen vacancies by reduction treatment generate local states below the conduction band edge and extend the light absorption of TiO2 nanoparticles from the UV to the visible region(28,29).

Table 3: calculated band gap of prepared and modified tio2

Sample	Energy gap (ev)
A-TiO2	3.2
R-TiO2	2.78
T-K-600	2.43
T-Na-600	2.4
T-K-850	2.04
T-Na-850	2.02

The nanoparticles grin size and the surface morphology of prepared and modified tio2 were analyzed by atomic force microscopy (AFM). figs.(5-7) show the AFM 2D images of prepared and modified tio2 nanoparticles, we can note that the as-prepare TiO2 nanoprticles has a uniform and smooth surface. Also, the grain size of modified TiO2 appears smaller than that as-prepared tio2 as shown in table 4, contrary, the surface roughness parameters of modified tio2 larger than that unmodified tio2, this can explained by the formation of oxygen vacancies (30).

Table 4 : roughness values and grain size of as-prepared and modified tio2

compound	Surface roughness Ra nm	Root mean square RMS nm	Grain size nm
R-TiO2	0.925	1.117	114.8
A-TiO2	0.911	1.145	80.76
T-K-850	0.948	1.163	81.35
T-K-600	1.073	1.396	74.16
T-Na-850	1.662	1.979	81.22
T-Na-600	1.679	2.102	44.72

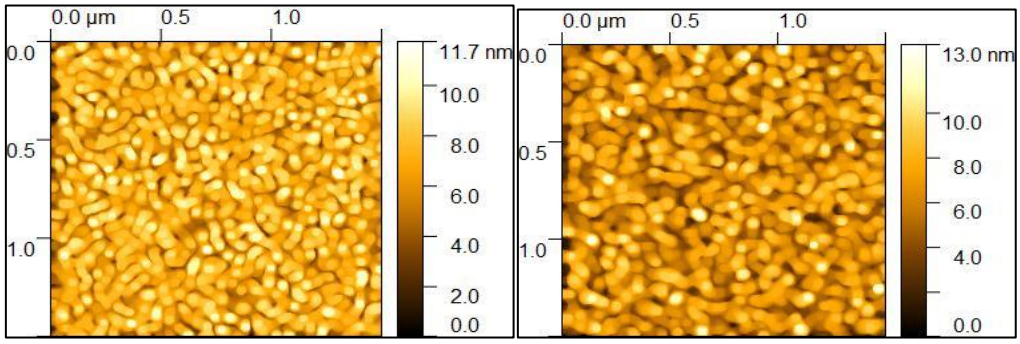

Figure 5 :1.5 x 1.5um 2D AFM images of R-TiO2(left) and A-TiO2 (right)

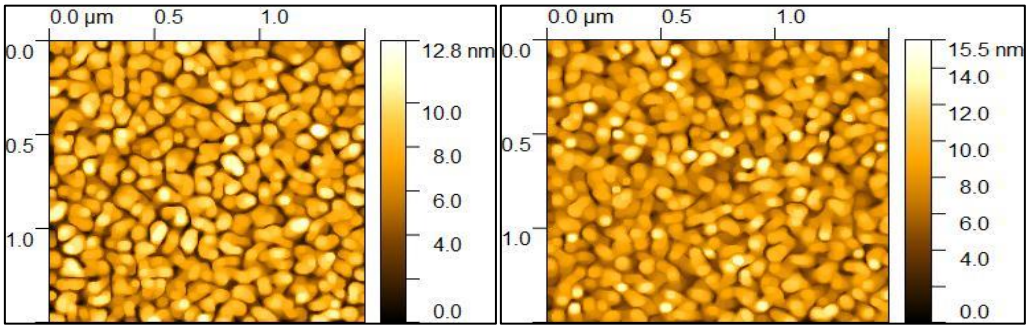

Figure 6 : .5 x 1.5um 2D AFM images of T-K-850(left) and T-K-600 (right)

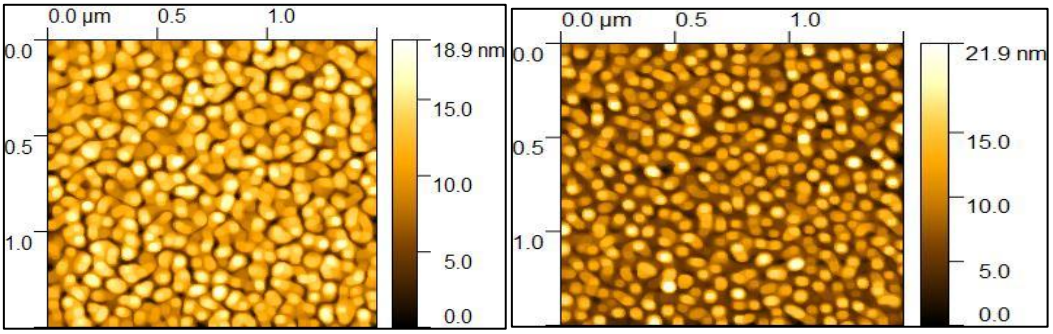

Figure 7: 1.5x1.5um 2D AFM images of T-Na-850(left) and T-Na-600 (right)

The elemental structure of as-prepared and modified TiO2 was done using

Energy Dispersive Spectroscopy (EDS), as shown in figs. (8-10), The Ti and O peaks can be found in all EDS spectra without any other peaks, this indicate that the as-prepared and modified TiO2 nanoparticles are pure and successfully removal of unreacted reducing agents after reduction treatment.

We can calculate the stoichiometry of all compounds from the atomic and weight percentage values(insets in figures 8-10), as we can note from table 5, the stoichiometry of as-prepared compounds match the standard chemical formula of TiO2,while the oxygen vacancies formation as a result of reduction treatment make the resulted compounds nonstoichiometry. Generally, EDS measurements confirms the formation of defective TiO2 nanoparticles after the reduction treatment which implying the presence of defective TiO2-x layer surrounding the TiO2 core (31).

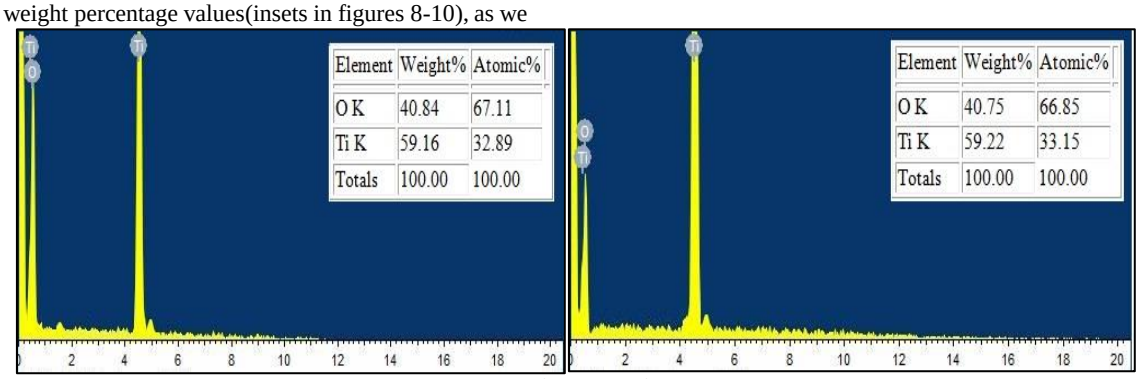

Figure 8 : EDS spectra of A-TiO2(left) and R-TiO2 (right)

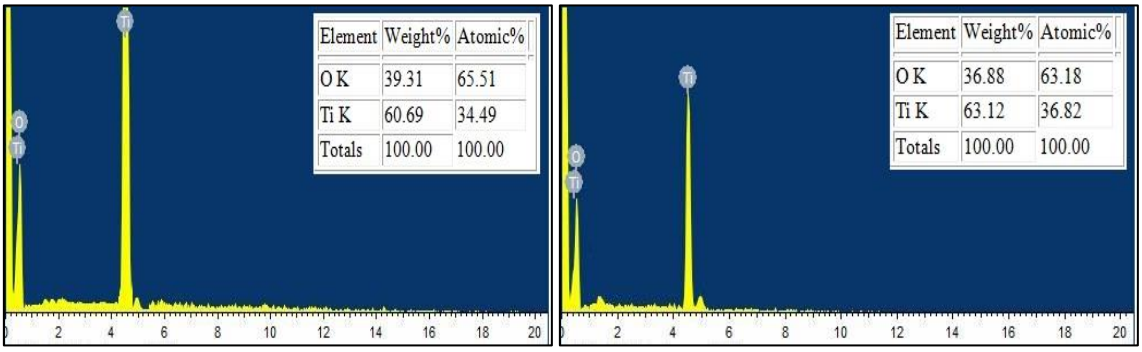

Figure 9 : EDS spectra of T-K-600(left) and T-K-850 (right)

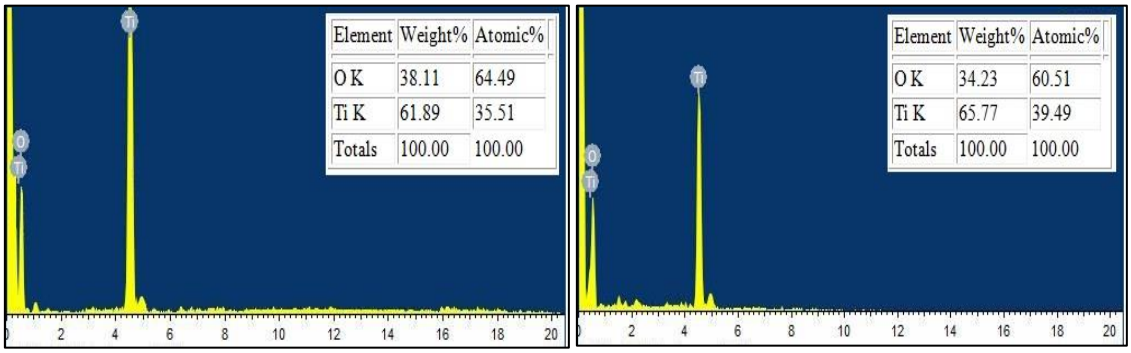

Figure 10 : EDS spectra of T-Na-600(left) and T-Na-850 (right)

Table 5 : calculated chemical formula

Compound	Formula
A-TiO2	TiO2
R-TiO2	TiO2
T-K-600	TiO1.89
T-Na-600	TiO1.81
T-K-850	TiO1.71
T-Na-850	TiO1.53

3.1 Computational details

To obtain the relaxed structures, we used the SIESTA implementation of density functional theory (DFT) to optimise the structures using, LDA, the local density approximation with the Ceperley-Alder exchange correlation functional and, DZP, double zeta polarized basis set [241] The initial unit cells were relaxed until the forces on the atoms are minimised to below 0.01 eV $Å^{-1}$. Results are obtained for the electronic density of states (DOS).

3.2. Oxygen vacancies in anatase TiO2

To examine the effect of oxygen vacancies in anatase TiO_2, we relax a super unit cell of ideal TiO_2 which contains 72 atoms (48 oxygen atoms and 24 titanium atoms) to obtain the relaxed structure, then we calculate the density of states, DOS. Later we simulate three different super unit cells; first we remove one oxygen atom from the unrelaxed super unit cell (71 atoms) and then optimize it, second we remove two oxygen atoms from the initial super unit cell (70 atoms) and relax it, and finally we remove three oxygen atoms from the initial super cell (69 atoms) and relax it. For all the three different unit cells, we calculate the density of states.

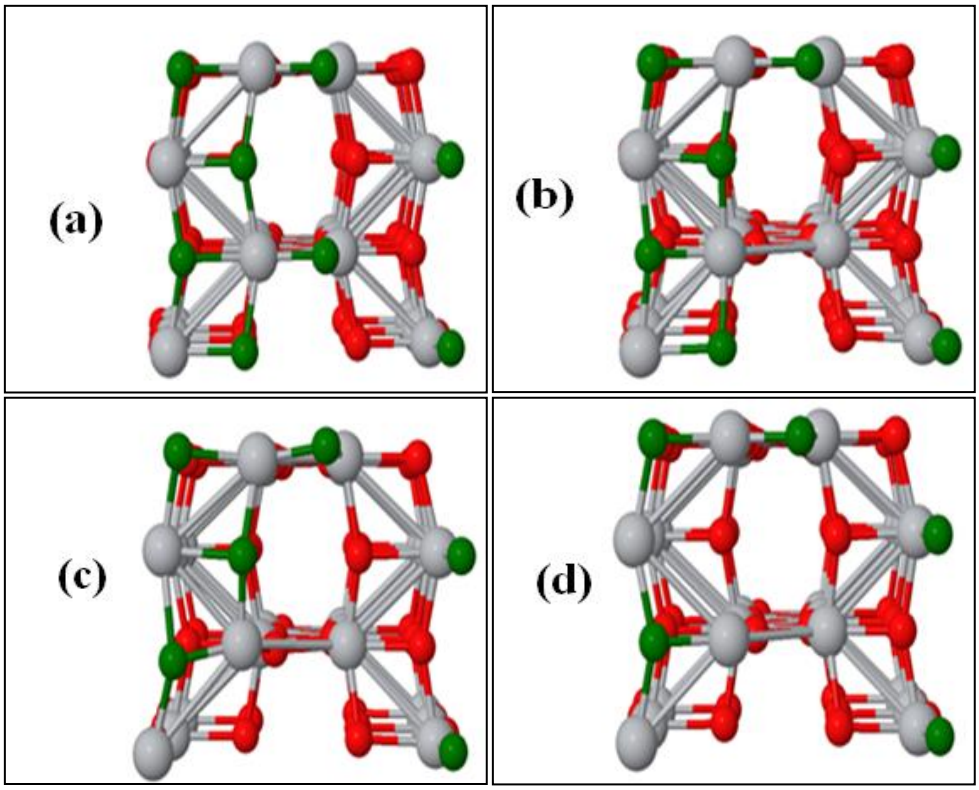

Figure (11) Relaxed structure geometries of (a): anatase TiO_2, (b-d): TiO_2 anatase with one, two and there oxygen vacancies respectively. Large gray sphere and small red sphere represent Ti and O atoms reactively, green colour sphere denoted to O surface atoms.

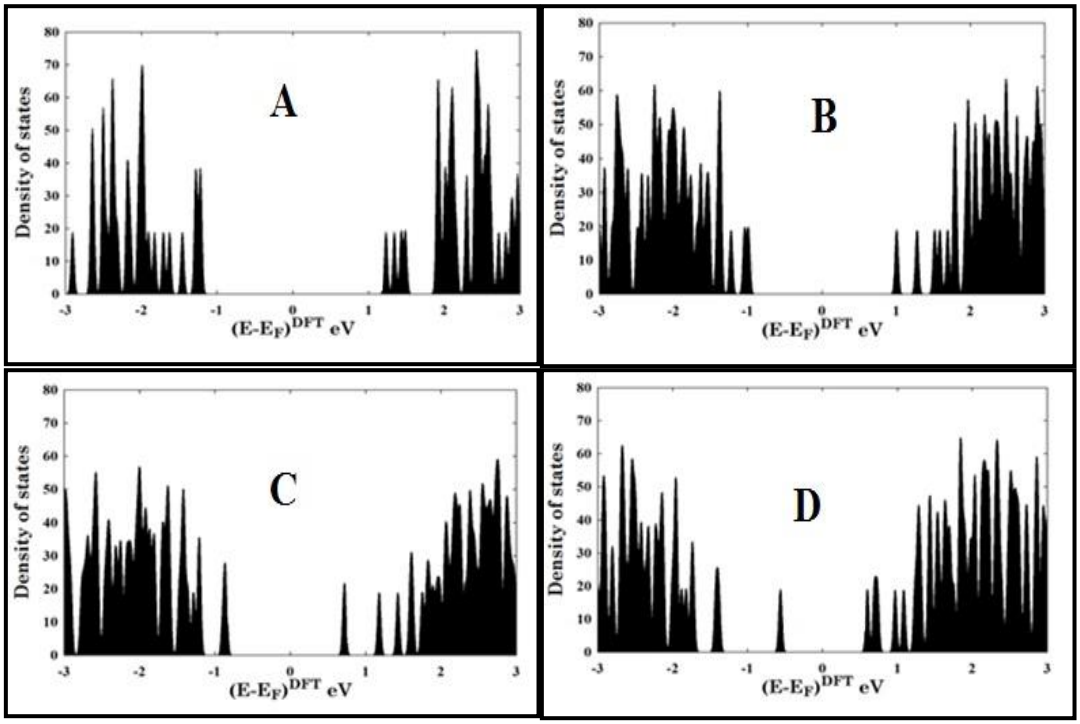

Figure (12) DOS of (a): anatase TiO_2, (b-d): TiO_2 anatase with one, two and there oxygen vacancies respectively.

3.3 Oxygen vacancies in rutile TiO_2

To examine the effect of oxygen vacancies in rutile TiO_2, we relax a super unit cell of ideal TiO_2 which contains 24 atoms (16 oxygen atoms and 8 titanium atoms) then we repeat the same strategy that used in case of anatase TiO_2 by removing one, two and three oxygen atoms from the initial unit cells.

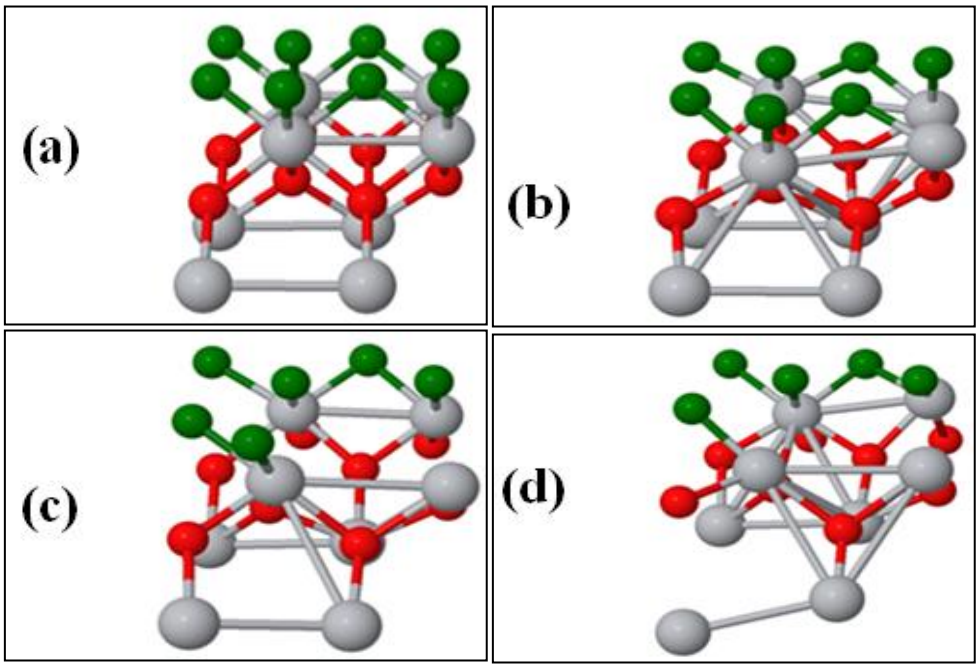

Figure (13) Relaxed structure geometries of (a): Rutile TiO_2, (b-d): TiO_2 rutile with one, two and there oxygen vacancies respectively. Large gray sphere and small red sphere represent Ti and O atoms reactively, green colour sphere denoted to O surface atoms.

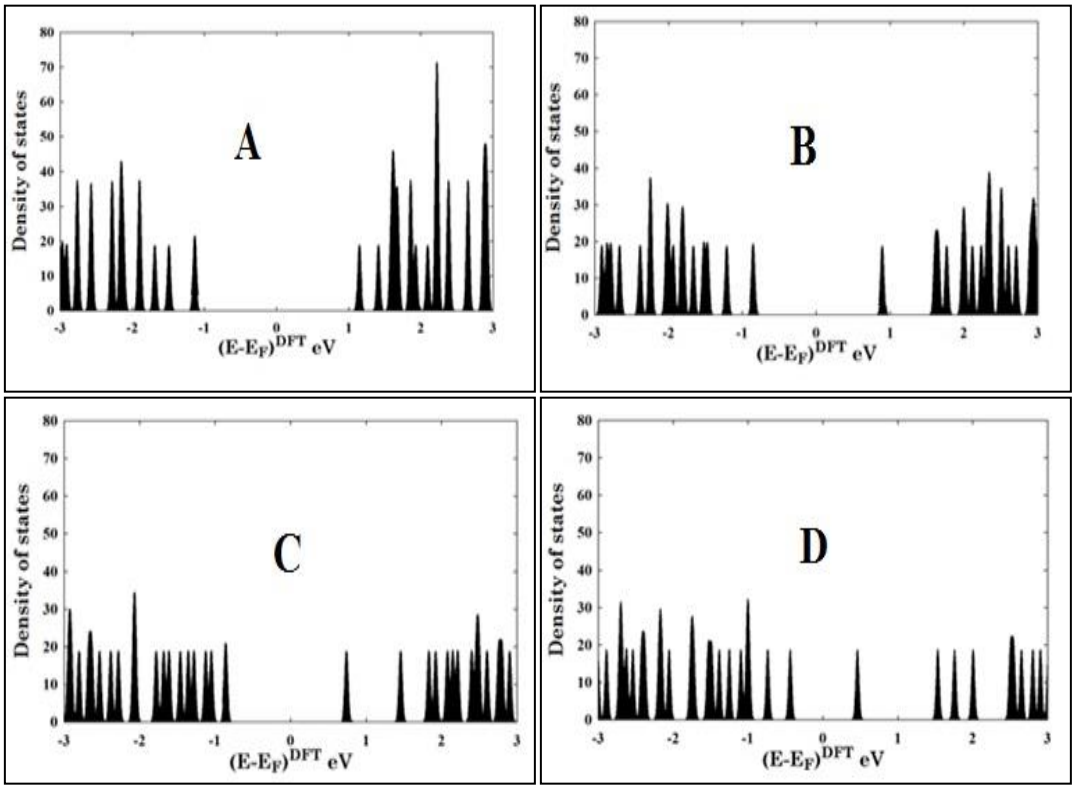

Figure (14) DOS of (a): Rutile TiO_2, (b-d): TiO_2 rutile with one, two and there oxygen vacancies respectively**.**

3.4 Electronic properties:

Due to the importance of anatase and rutile TiO_2 energy gap for different applications, the (Eg) of pristine and reduced TiO_2 were extracted from DOS plots figures (12) and (14) and the results are summarized in table (6). The results shows that the calculated energy gap of pristine anatase and rutile TiO2 is about 2.65 and 2.28 eV respectively, which is underestimated by approximately one third comparing with the experimental values of 3.2 and 2.78 eV for anatase and rutile respectively. This remarkable discrepancy between experimental and theoretical studies can be observed due to the known limitation of the DFT theory. Many publications reported that the DFT theory calculation lowered the energy by about 30% compared with the experimental value [242-247].
As the number of removed oxygen atoms increase, the energy gap values deeply decreased, hence removing three oxygen atoms from the structures lead to remarkably reduce in the energy gap from 2.65 eV to 1.161 eV and from 2.28 eV to 0.747 eV for anatase and rutile TiO_2 respectively.

Table (6): Calculated energy gaps (eV) for all TiO_2 structures.

Oxygen removed	Eg (eV)			
	Pristine	1 O	2 O	3 O
Anatase	2.650	1.996	1.571	1.161
Rutile	2.280	1.672	1.328	0.747

However, the decrease in the energy gap can be explained by the formation of oxygen vacancies, the results of DOS (figures 12 and 14) indicate that the vacancy band created below the conduction band minimum (CBM) as a result of the formation of oxygen vacancy. As the oxygen vacancy concentration increase, the vacancy band shifts deeper below the CBM [248].
According to the above theoretical results, we can conclude that the structures with two oxygen vacancies are closed to our experimental study for reduced TiO_2 taking into account the previously mentioned DFT limitation.

4. Conclusions

In this work, reduced TiO2 nanoparticles were synthesized using sold state reaction of as-prepared TiO2 with NaAlH4 and KBH4 as a reducing agents. The structural properties analyzed by XRD show a slightly difference from the as-prepared TiO2 but have the same antase and rutile phases, the line broadening and larger diffraction angles of reduced TiO2 related to the formation of oxygen vacancies. The results of morphology analysis indicate that the reduced TiO2 have a surface roughness larger than of as-prepared TiO2 and the grain size decreased after reduction treatment. The purity of prepared and reduced TiO2 confirmed by EDS analysis and only Ti and O founded in the spectra , the stoichiometry calculations indicate formation TiO2 with oxygen deficient which also indicate formation oxygen vacancies in resulted oxide. Band gap measurement improves that the reduction treatment shifts the absorption spectra of reduced TiO2 from ultraviolet to the visible light region.

References

[1] J. Yu, J. Low, W. Xiao, P. Zhou, M. Jaroniec, Enhanced photocatalytic CO2-reduction activity of anatase TiO2by coexposed {0 0 1} and {1 0 1} facets,J. Am. Chem. Soc. 136 (2014) pp.8839–8842.

[2] A.A. Ashkarran, H. Hamidinezhad, H. Haddadi, M. Mahmoudi, Double-dopedTiO2nanoparticles as an efficient visible-light-active photocatalyst andantibacterial agent under solar simulated light, App. Surf. Sci. 301 (2014) pp.338–345.

[3] J. Tian, Z. Zhao, A. Kumar, R.I. Boughton, H. Liu, Recent progress in design, synthesis, and applications of one-dimensional TiO2nanostructured surfaceheterostructures: a review, Chem. Soc. Rev. 43 (2014) pp.6920–6937.

[4] A. Testino, I. R. Bellobono, V. Buscaglia, C. Canevali,M. D'Arienzo, S. Polizzi, R. Scotti and F. Morazzoni, Optimizing the photocatalytic properties of hydrothermal TiO2 by the control of phase composition and particle morphology. a systematic approach., J. Am.Chem. Soc., (2007),pp.129, 3564.

[5] J. Su, X. Zou, G.-D. Li, Y.-M. Jiang, Y. Cao, J. Zhao and J.-S. Chen, Room-temperature spontaneous crystallization of porous amorphous titania into a high-surface-area anatase photocatalyst., Chem. Commun., (2013), pp.49, 8217.

[6] J. Pan, G. Liu, G. Q. Lu and H. M. Cheng, On the True Photoreactivity Order of {001}, {010}, and {101} Facets of Anatase TiO_2 Crystals, Angew. Chem., Int.Ed., (2011),pp. 50, 2133.

[7] X. Zou, R. Silva, X. Huang, J. F. Al-Sharab and T. Asefa, A self cleaning porous TiO2-Ag core-shell nanocomposite material for surface enhanced Raman scattering, Chem. Commun., (2013),pp. 49, 382.

[8] H. G. Yang, C. H. Sun, S. Z. Qiao, J. Zou, G. Liu, S. C. Smith,H. M. Cheng and G. Q. Lu, Anatase TiO_2 single crystals with a large percentage of reactive facets ,Nature, (2008),pp.453, 638.

[9] L. Wang, T. Sasaki, Titanium oxide nanosheets: graphene analogues withversatile functionalities, Chem. Rev. 114 (2014) pp.9455–9486.

[10] Y. Wang, J. Yu, W. Xiao, Q. Li, Microwave-assisted hydrothermal synthesis of graphene based Au–TiO2 photocatalysts for efficient visible-light hydrogen production, J. Mater. Chem. A 2 (2014) pp.3847–3855.

[11] R. Sasikala, A. Shirole, V. Sudarsan, T. Sakuntala, C. Sudakar, R. Naik, Highly dispersed phase of SnO2 on TiO2 nanoparticles synthesized by polyol-mediated route: Photocatalytic activity for hydrogen generation Int. J. Hydrogen Energy 34, (2009) pp.3621-3630.

[12] D. C. Cronemeyer, Infrared Absorption of Reduced Rutile TiO2 Single Crystals, Phys. ReV. 113(1959) 1222.

[13] Designed Self-Doped Titanium Oxide Thin Films for Efficient Visible-Light Photocatalysis, I. Justicia, P. Ordejon, G. Canto, J. L. Mozos, J. Fraxedes, G. A. Battiston, R. Gerbasi, A. Figueras, AdV. Mater. (2002) pp.14, 1399

[14] F. Zuo, L. Wang, T. Wu, Z. Zhang, D. Borchardt, P. Feng, Self-Doped Ti3+ Enhanced Photocatalyst for Hydrogen Production under ,J. Am. Chem. Soc. 132(2010) pp.11856– 11857 .

[15] Z. Zheng, B. Huang, X. Meng, J. Wang, S. Wang, Z. Lou,Z. Wang, X. Qin, X. Zhang and Y. Dai, Metallic zinc-assisted synthesis of Ti 3+ self doped TiO 2 with tunable phase composition and visible-light photocatalytic activity, Chem. Commun., (2013) pp.49, 868.

[16] F. N. Sayed, O. D. Jayakumar, R. M. Kadam, S. R. Bharadwaj,L. Kienle, U. Sch¨urmann, S. Kaps, R. Adelung, J. P. Mittal andA. K. Tyagi, Photochemical Hydrogen Generation Using Nitrogen-Doped TiO2–Pd Nanoparticles: Facile Synthesis and Effect of Ti3+ Incorporation, J. Phys. Chem. C, (2012) pp.116, 12462.

[17] C. Yang, Z. Wang, T. Lin, H. Yin, X. Lu, D. Wang, T. Xu, C. Zheng, J. Lin, F. Huang, X. Xie and M. Jiang, Core-shell nanostructured "black" rutile titania as excellent catalyst for hydrogen production enhanced by sulfur doping, J. Am.Chem. Soc., (2013) pp.135, 17831.

[18] Q. Kang, J. Cao, Y. Zhang, L. Liu, H. Xu and J. Ye, Reduced TiO_2 nanotube arrays for photoelectrochemical water splitting, J. Mater.Chem. A, (2013) pp. 1, 5766.

[19] X. Zou, J. Liu, J. Su, F. Zuo, J. Chen and P. Feng, Facile Synthesis of Thermal- and Photostable Titania with Paramagnetic Oxygen Vacancies for Visible-Light Photocatalysis ,Chem. – Eur.J., (2013) pp.19, 2866.

[20] F. Zuo, L. Wang, T. Wu, Z. Zhang, D. Borchardt and P. Feng, Self Doped Ti^{3+} Enhanced Photocatalyst for Hydrogen Production under Visible Light,J. Am. Chem. Soc., (2010) pp.132, 11856.

[21] N. Liu, V. Haublein, X. Zhou, U. Venkatesan, M. Hartmann, M. Mackovic,T. Nakajima, E. Spiecker, A. Osvet, L. Frey, P. Schmuki, "Black" TiO2 nanotubes formed by high-energy proton implantation show Noble-metal-co-catalyst free photocatalytic H2-evolution, Nano Lett. 15 (2015) pp. 6815–6820.

[22] S.G. Ullattil, P. Periyat, A 'one pot' gel combustion strategy towards Ti3+ self-doped 'black' anatase TiO2 - x solar photocatalyst, J. Mater. Chem. A 4 (2016) pp.5854–5858.

[23] J.H. Pan, Z.Y. Cai, Y. Yu, X.S. Zhao, Controllable synthesis of mesoporous F-TiO2 spheres for effective photocatalysis, J. Mater. Chem. 21(2011) pp. 11430.

[24] X. Chen, L. Liu, Z. Liu, M. A. Marcus, W. Wang, N. A. Oyler, M. E. Grass, B. Mao, P. Glans, P. Y. Yu, J. Guo, S. S. Mao, Properties of Disorder-Engineered Black Titanium Dioxide Nanoparticles through Hydrogenation, Scientific Reports,3(2013) pp.1510.

[25] W. Wang, Y. Ni, C. Lu and Z. Xu, hydrogenation of TiO2 nanosheets with exposed {001} facets for enhanced photocatalytc activity, RSC Adv., 2(2012) pp. 8286.

[26] Z. Wang, C. Yang, T. Lin, H. Yin, P. Chen, D. Wan, F. Xu, F. Huang J. Lin, X. Xiec, M. Jiangc, Visible-light photocatalytic, solar thermal and photoelectrochemical properties of aluminium-reduced black titania, Energy Environ. Sci., 6(2013) pp. 3007.

[27] Y. Jiang, F. Li, Y. Liu, Y. Hong, P. Liu, L. Ni, Construction of TiO2 hollow nanosphere/g -C3N4 composites with 2 superior visible-light photocatalytic activity and mechanism insight, Ind. Eng. Chem. Res. 41(2016) pp.130-141.

[28] X.Y. Pan, M.-Q. Yang, X.Z. Fu, N. Zhang, Y.-J. Xu, Defective TiO2 with oxygen vacancies: synthesis, properties and photocatalytic applications, Nanoscale, 5 (2013) pp.3601–3614.

[29] B. Bharti, S. Kumar, H.-N. Lee and R. Kumar, Formation of oxygen vacancies and Ti3+ state in TiO2 thin lm and enhanced optical properties by air plasma treatment, Sci. Rep.,6 (2016) pp.32355.

[30] V. Gurylev, C.Y. Su and T.P. Perng, Surface reconstruction, oxygen vacancy distribution and photocatalytic activity of hydrogenated titanium oxide thin film, Journal of Catalysis, 330 (2015) pp.177–186.

[31] M. W. Shah, Y. Zhu, X. Fan, J. Zhao, Y. Li, S. Asim, C. Wang, Facile Synthesis of Defective TiO2−x Nanocrystals with High Surface Area and Tailoring Bandgap for Visible-light Photocatalysis, Scientific reports 5, (2015) pp.15804.

[32] Soler, J. M., Artacho, E., Gale, J. D., García, A., Junquera, J., Ordejón, P., & Sánchez-Portal, D. The SIESTA method for ab initio order-N materials simulation. *Journal of Physics: Condensed Matter*, *14*,11 (2002) pp.2745.

[33] Yang, K., Dai, Y., & Huang, B. Study of the nitrogen concentration influence on N-doped TiO2 anatase from first-principles calculations. *The journal of physical chemistry C*, *111*(32). (2007). pp.12086-12090.

[34] Wan, L., Li, J. F., Feng, J. Y., Sun, W., & Mao, Z. Q. Anatase TiO2 films with 2.2 eV band gap prepared by micro-arc oxidation. *Materials science and engineering: B*, *139*(2-3), (2007) pp.216-220.

[35] Zhang, Y. F., Lin, W., Li, Y., Ding, K. N., & Li, J. Q. A Theoretical Study on the Electronic Structures of TiO2: Effect of Hartree− Fock Exchange. *The Journal of Physical Chemistry B*, *109*,41 (2005) pp.19270-19277.

[36] Glassford, K. M., & Chelikowsky, J. R. Structural and electronic properties of titanium dioxide. *Physical Review B*, *46*,3 (1992) pp.1284.

[37] Yang, K., Dai, Y., Huang, B., & Whangbo, M. H. Density functional characterization of the band edges, the band gap states, and the preferred doping sites of halogen-doped TiO2. *Chemistry of Materials*, *20*,20 (2008) pp.6528-6534.

[38] Su, R., Tiruvalam, R., He, Q., Dimitratos, N., Kesavan, L., Hammond, C., ... & Besenbacher, F. Promotion of phenol photodecomposition over TiO2 using Au, Pd, and Au–Pd nanoparticles. *ACS nano*, *6*,7 (2012) pp.6284-6292.

[39] Janotti, A., Varley, J. B., Rinke, P., Umezawa, N., Kresse, G., & Van de Walle, C. G. Hybrid functional studies of the oxygen vacancy in TiO 2. *Physical Review B*, *81*,8 (2010) pp.085212.